On the role of crystal and stress anisotropy in magnetic Barkhausen noise

Meisam Sheikh Amiri[a,*], Matthias Thielen[b], Madalina Rabung[c], Michael Marx[b], Klaus Szielasko[c], Christian Boller[a,c]

[a] Saarland University, Chair in Nondestructive Testing and Quality Assurance, Campus E3 1, 66123 Saarbrücken, Germany

[b] Saarland University, MWW, Campus E3 1, 66123 Saarbrücken, Germany

[c] Fraunhofer Institute for Nondestructive Testing (IZFP), Campus E3 1, 66123 Saarbrücken, Germany

Dedicated to the 60th Anniversary of Dr. Iris Altpeter

1. Abstract

The article describes the micromagnetic behavior of non- and pre-plastically deformed high strength steel samples under applied stress using different magnetic nondestructive methods such as magnetic Barkhausen noise analysis and hysteresis measurements. It was found that the maximum amplitude of Barkhausen noise (M_{MAX}) increases with applied stress up to a certain point and then decreases again (so-called $M_{MAX}(\sigma)$-curve). Changes of magnetostriction, hysteresis curves and magnetic domain structures have been measured and have been further investigated to find out the reasons with respect to macro- and microscopic material behavior. The results obtained are mainly discussed on the basis of the Villari effect and the relation between applied stress and the Barkhausen noise parameters is described. It is concluded that the interaction between crystal and stress anisotropy is the main reason of the specific $M_{MAX}(\sigma)$-curve observed.

Key words: Applied and residual stress, Barkhausen noise, Magnetic force microscopy

* Corresponding author: Tel. +49 (0) 681 9302 3831 / Email address: Meisam.SheikhAmiri@izfp.fraunhofer.de

2. Introduction

The effect of applied and residual stress on magnetic Barkhausen noise (MBN) has been a subject of research in the past [1-3]. Karjalainen et al. have studied the influence of tensile and cyclic loading on Barkhausen noise [4]. They have demonstrated that the sensitivity of Barkhausen noise in a material's elastic strain range is much less than in the plastic one. They have also shown that the yield point is detectable with MBN. Jagadish et al. investigated the effect of the uniaxial stress on MBN [5]. They have shown that applied tensile stress increases MBN while compressive stress decreases it. Stefanita et al. have investigated MBN under plastic and elastic strain [6]. They have shown that the effects of elastic strain are much higher than those of plastic strain. Moreover the authors have proposed that elastic deformation creates a new easy axis which is the reason of MBN behavior under elastic strain while pinning of dislocations, changing of crystal easy axis and local elastic strain are three possibilities of how plastic deformation could change MBN. Sablik has proposed a model for simulating the dependence of the maximum MBN signal versus applied stress [7]. He has also demonstrated on the basis of a model that the maximum of MBN increases with increasing applied tensile stress. Lindgren et al. studied the effect of pre-straining and residual stress in soft-magnetic and duplex steel, respectively [8, 9]. They have shown that pre-straining generates compressive and tensile residual stress parallel and perpendicular to the loading direction, respectively, in a soft-magnetic steel that can be detected by MBN. Interestingly they have reported that tensile pre-straining in the Lüders band zone induces tensile residual stress in the loading direction which leads to increasing MBN activity. Kleber et al. have also reported those results in Armco iron, but they have shown that in low carbon steel MBN decreases with increasing plastic deformation more than 1% strain, however a small increase in MBN amplitude is visible in their results but has been neglected [10]. Finally they have concluded that the underlying of dislocation tangles and residuals stresses are the cause of the different behavior of Armco iron and the low carbon steel after 1% tensile plastic deformation. Piotrowski et al., also investigated plastic deformation, obtained from cold rolling and tensile deformation, in Armco steel using MBN [11]. They also compared the results of MBN with magnetoacoustic emission (MAE). They reported that MBN and MAE increases with deformation up to maximum and then decreases again. As a reason they mentioned that the role of dislocation tangles are more dominant comparing to the influence of plastic deformation and residual stresses. More recently, Altpeter et al. measured micro residual stresses of the 2nd and 3rd order using MBN analysis [12]. They found for WB 36 steel that M_{MAX} increases with increasing applied stress up to a certain stress and then

decreases again. They also showed that an increase in tensile residual stress shifts the maximum of the M_{MAX} (σ) curve to the smaller applied stresses values (and vice versa for compressive stress).

So far not too much has been published on trying to generalize the MBN behavior under the effect of applied and residual stresses on a macro- as well as a microscopic scale. Major knowledge in that regard can be found in textbooks such as from Cullity [2]. When trying to determine a unit onto which the effect of stress on a domain wall behavior can be reduced best such that the resulting electromagnetic principle can be generalized best the smallest common 'denominator' turns out to be a material's single crystal. Figure 1a shows symbolically a single crystal comprising four domains in an unstressed state. A small tensile stress will lead the domain walls to move in such a way that the domains magnetized rectangular to the stress directions will be reduced because these domains have a high magnetoeleastic energy (Figure 1b). These domains will even fully vanish when the applied tensile stress has reached a certain level and remaining magnetoelastic energy turns to a minimum (Figure 1c). Only a small additional applied field is now required to fully saturate the specimen because the transition can be achieved by a simple 180° wall motion (Figure 1d). When a compressive stress is applied to the crystal (Figure 2a), then the domains in the direction of the stress will gradually vanish (Figure 2b and c) and a much higher electromagnetic field has to be applied in case a fully saturated crystal is intended to be achieved (Figure 2d).

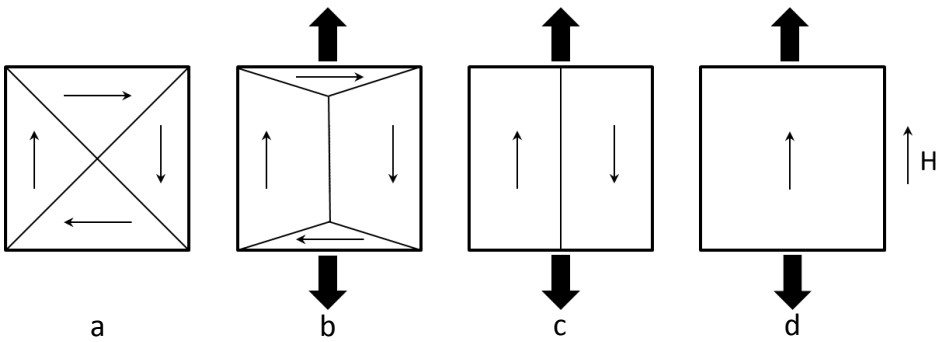

Figure 1: Schematic magnetization of a material with positive magnetostriction under tensile stress.

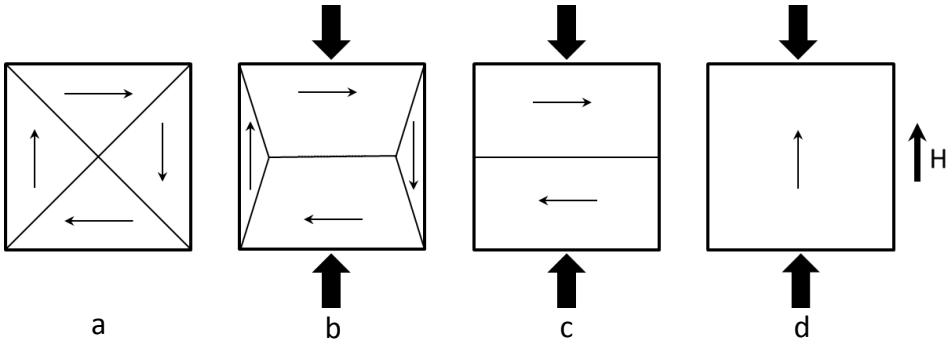

Figure 2: Schematic magnetization of a material with positive magnetostriction under compressive stress.

The type of crystal and its orientation can therefore become the building block on how to understand a structural material's as well as component's stress behavior based on MBN measurements or to interpret MBN measurement results when stresses in a material and/or structure are known. Based on this model results observed and described throughout the following will be tried to be explained and hence interpreted.

The MBN activity depends on the magnetic domain structure and the movement of magnetic domain walls where the energy equilibrium between domains controls the structure and activity of domain walls. Magnetoelastic energy, which reflects the effect of stress on the domain structure, strongly affects the domain structure and domain wall movement. To this end, the behavior of MBN under influence of applied and residual stress has been studied and reasons have also been deeply investigated based on hysteresis curves, magnetostriction measurements and domain structure imaging.

3. Sample preparation and experimental method

The study has been carried out on high strength steel for structural application. Figure 3 shows that the microstructure of high strength steel is fully martensitic.

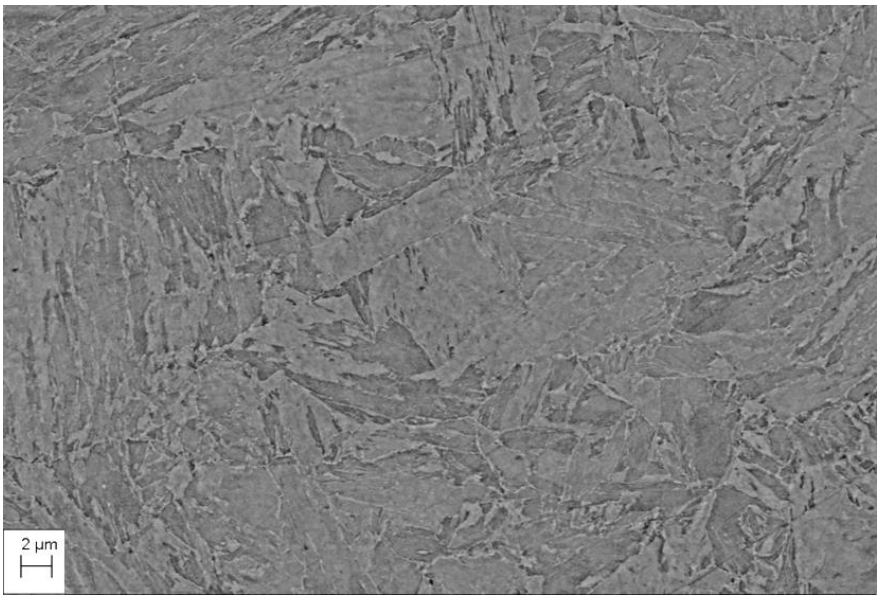

Figure 3: SEM image of microstructure of high strength steel for structural application. Polished and etched in Nital.

First, five small tensile test specimens (thickness 2 mm, gauge length 20 mm, width 4 mm) were cut. Then, a tensile test was performed on one of the samples to determine the yield stress (Figure 4).

Thereafter micro residual stresses were generated on two of the samples through plastic deformation up to 1% in plastic strain followed by unloading down to zero load (figure 4). The pre-straining was carried out with an Instron servo hydraulic tensile tester 8511.20 controlled by an MTS 6342F extensometer.

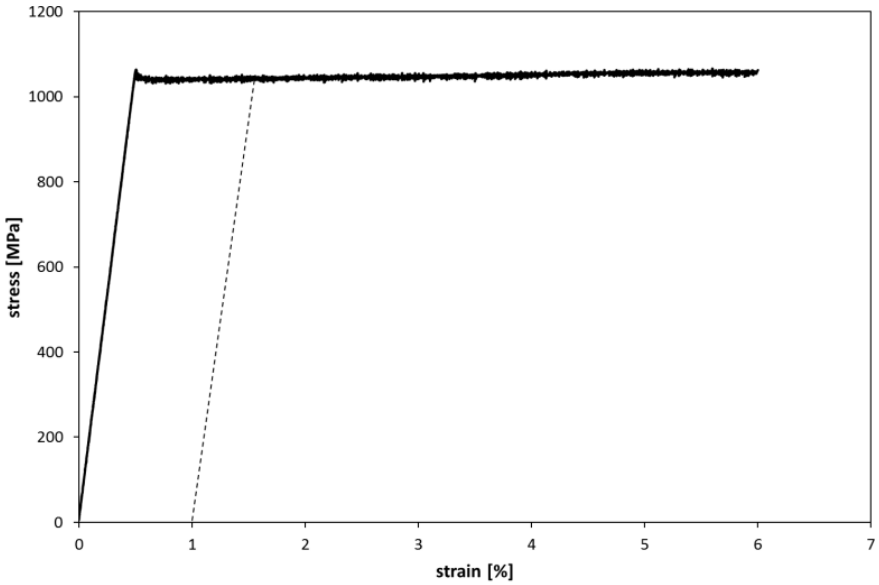

Figure 4: Stress-strain curve of a high strength steel for structural application.

In the next step MBN, the magnetic hysteresis curve and magnetostriction of the samples were measured using the Micromagnetic, Multiparameter, Microstructure and Stress Analysis (3MA) equipment [13], a B(H) measurement lab-setup and a strain gauge, respectively. Figure 5 shows the schematic experimental setup.

MBN was measured using a surface coil and the magnetic field strength (H) was measured using a Hall sensor (Figure 5). For the hysteresis measurements a coil wound around was used to pick up magnetic flux density (B) by integrating the induced voltage and a Hall sensor to measure the magnetic field strength (H). In order to measure magnetostriction of the samples a strain gauge was attached to the surface of the sample to measure the length changes (λ) resulting from the variation of the magnetic field (H) (Figure 5). An electromagnet was used in order to magnetize the sample from below the sample for all measurements mentioned above (Figure 5). Note that the magnetizing frequency and amplitude were different for each measurement. Samples were magnetized at 100 Hz and 15 A/cm for MBN measurement, at 1Hz for hysteresis curves and at 0.05 Hz for magnetostriction measurement while magnetization amplitude was 40 A/cm for both above mentioned measurements. Device limitation was the reason of choosing different frequency for different measurements.

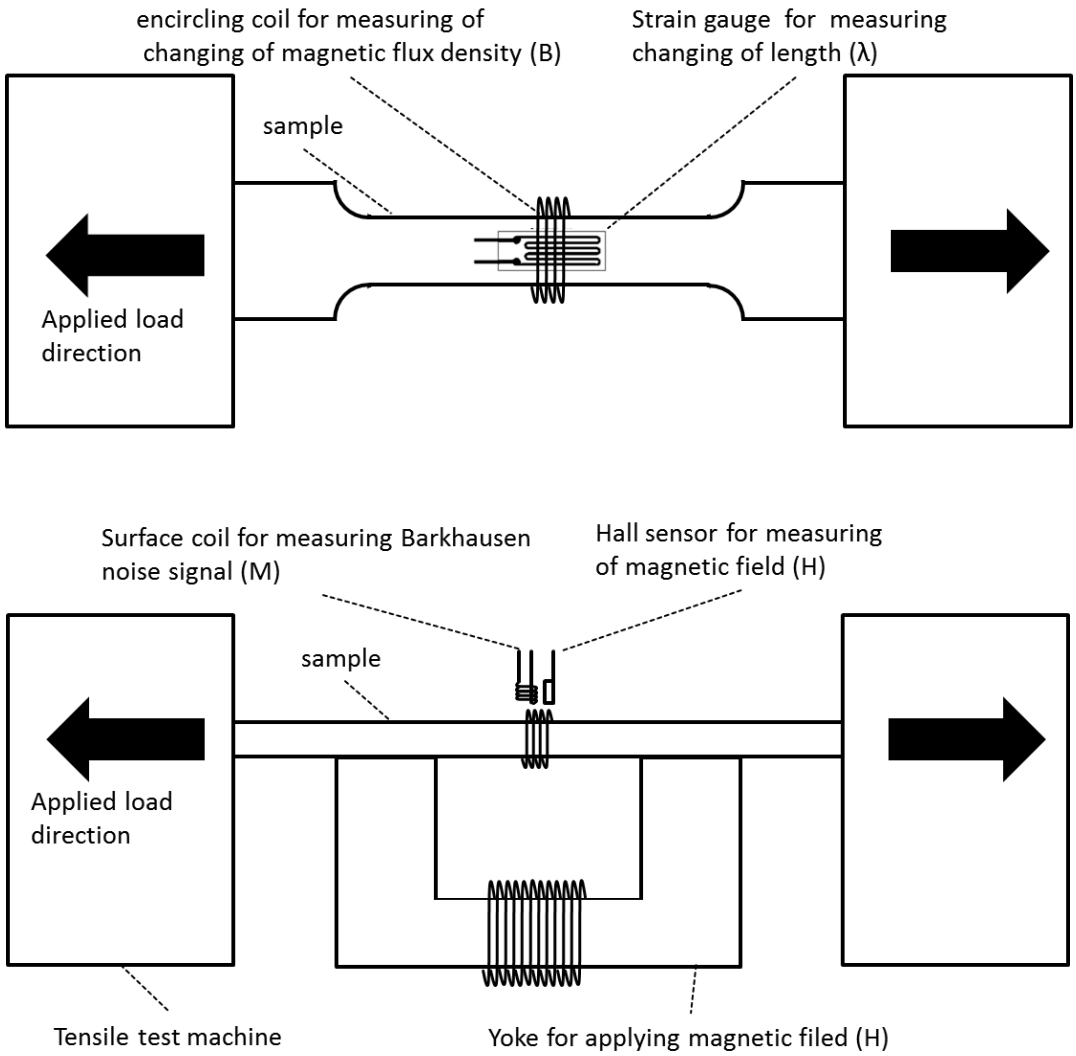

Figure 5: Experimental setup for measuring Barkhausen noise, hysteresis curves and magnetostriction (top and side view).

In order to better understand the behavior of MBN under applied stress, the domain structures under applied stress were investigated in an in-situ test using Magnetic Force Microscopy (MFM). To be sure that the measurements are always performed at the same location on the sample, a region was marked in the middle of the sample, where the stress field in the tensile test is supposed to be homogeneous. The marking was made with a focused ion beam (FIB) microscope at 20nA to receive a 40 × 40µm square with a depth of approx. 5µm. To minimize any topography effects the sample was then polished using a 0.25µm diamond suspension. After polishing topography of the sample was measured using an atomic force microscopy (AFM). The surface roughness was less than 5nm.

It should be noted that all measurements were carried out on non- and pre-plastically deformed samples in two stages: First under the absence of applied stress ($\sigma = 0$), and second under gradually ($\sigma_{step} = 50$ MPa) increasing applied stress. On the non-deformed samples only the effect of the applied stress on MBN was investigated. On the pre-deformed samples in the first stage just the effect of micro residual stress on MBN signal was considered, while at the second stage, the effect of residual as well as applied stress on MBN was studied. It is noteworthy that at the second stage, stress was applied up to half the yield strength.

4. Results and Discussion

4.1. Residual stress effect

Figure 6-8 show MBN, hysteresis and magnetostriction curves versus applied magnetic field amplitude, respectively.

Based on the fact that tensile plastic deformation generates micro compressive residual stresses after unloading, the results in Figure 6-8 can be described. The maximum amplitude of MBN (M_{MAX}) decreases and the magnetic coercive field at the maximum amplitude of Barkhausen noise (H_{CM}) increases with the generation of compressive micro residual stresses [3, 5]. The reason of this behavior is related to the activity of 90° and 180° domain walls in the presence of residual stress. Tensile residual stresses extend the 180° domain walls while compressive residual stresses extends 90° domain walls [1, 2]. Due to their elastic volume distortion the motion of 90° domain walls needs higher magnetic fields when compared to the 180° ones which is the reason why they are also known as the hardly movable domain walls. Since the MBN occurrence is directly related to the motion of domain walls, M_{MAX} decreases with increasing compressive micro residual stresses. Hysteresis curves also confirm the features of the MBN curves. As shown in Figure 7, the B(H) curve is widened with increasing compressive residual stresses while it narrows down when tensile residual stresses are present. In other words, compressive residual stress increases the coercive field (H_C) and decreases remnant flux density (B_r) [1, 2]. The effects of 90° domain walls are also visible in Figure 8. As previously described, they are acting as an obstacle for domain wall motion. This is also the main reason for different magnetostriction of non- and pre-deformed samples.

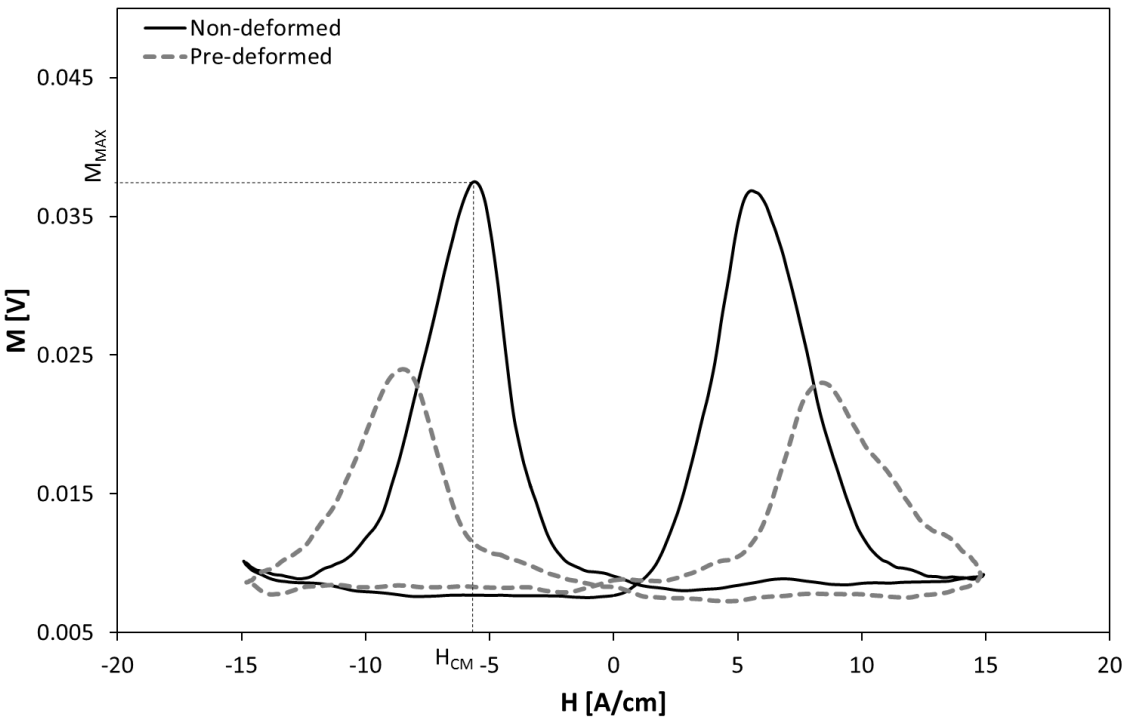

Figure 6 : Barkhausen noise signal for non- and pre-deformed sample.

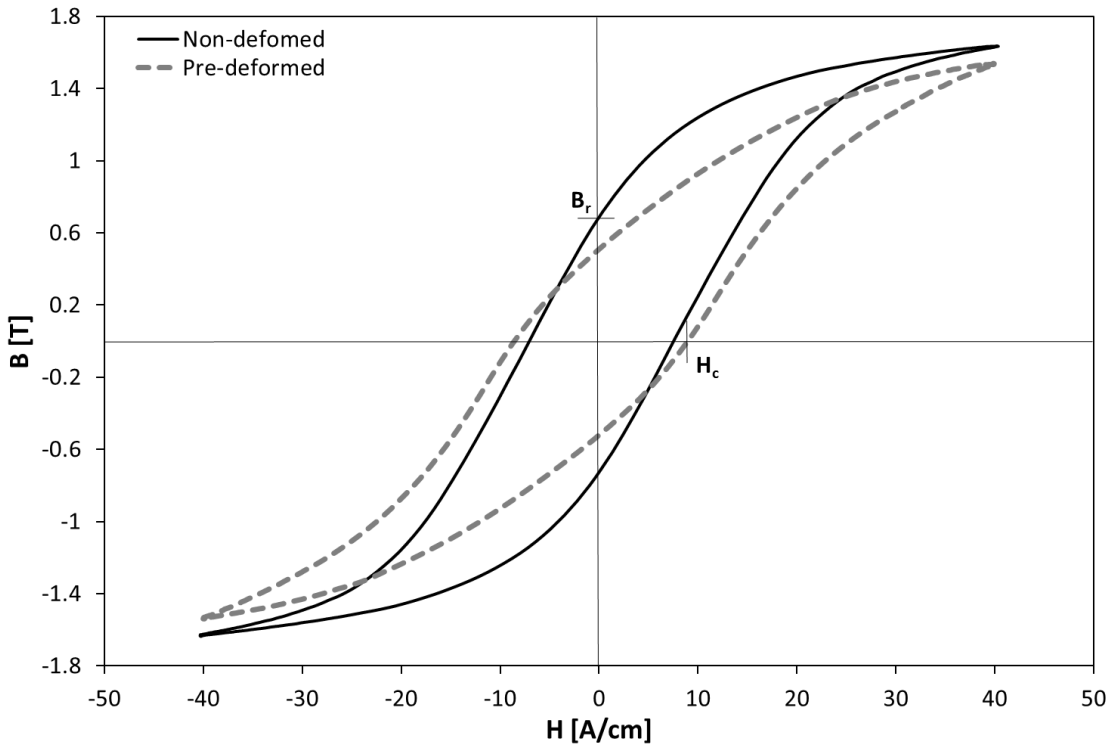

Figure 7 : Hysteresis curves for non- and pre-deformed sample.

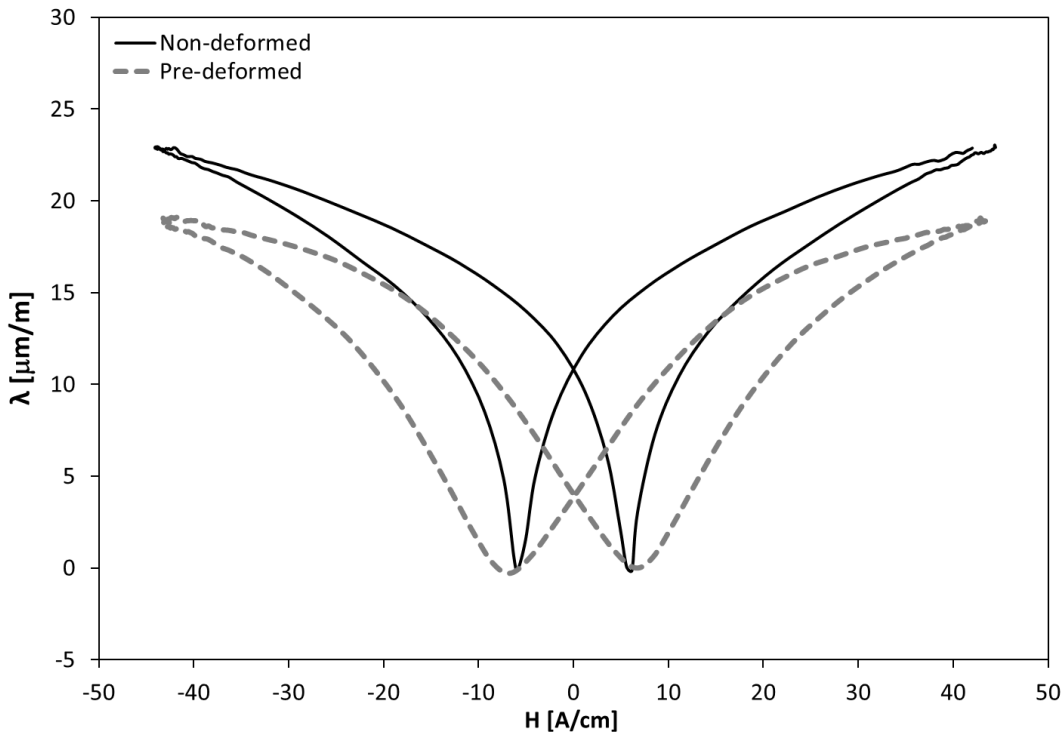

Figure 8 : Magnetostriction for non- and pre-deformed sample.

4.2. Applied stress effect

Figure 9 shows the relationship between applied stress and M_{MAX} as well as H_{CM} for the non-deformed sample. As can be seen M_{MAX} increases with increasing applied stress up to a certain point which is 150 MPa in the case considered here and then deceases again. As also expected H_{CM} decreased with increasing applied stress up to 150 MPa and then increased again. In order to better understand those observations, hysteresis measurements were carried out.

As Figure 10 demonstrates, B(H) curves show similar behavior under applied stress as MBN analysis, since B_r and H_C in the same sense to M_{MAX} and H_{CM} respectively (Figure 9 and 11). The behavior of B(H) curves under applied stress (Figure 10) can be described by means of Villari effect [14-16].

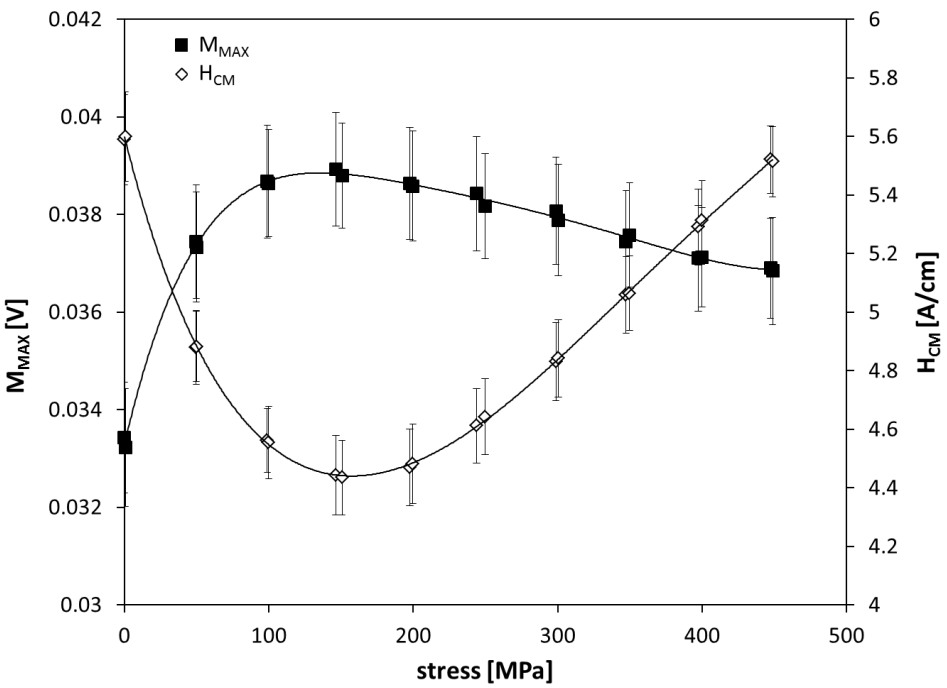

Figure 9: Relation between applied stress and maximum amplitude of MBN (M_{MAX}) and coercive field at the M_{MAX} (H_{CM}).

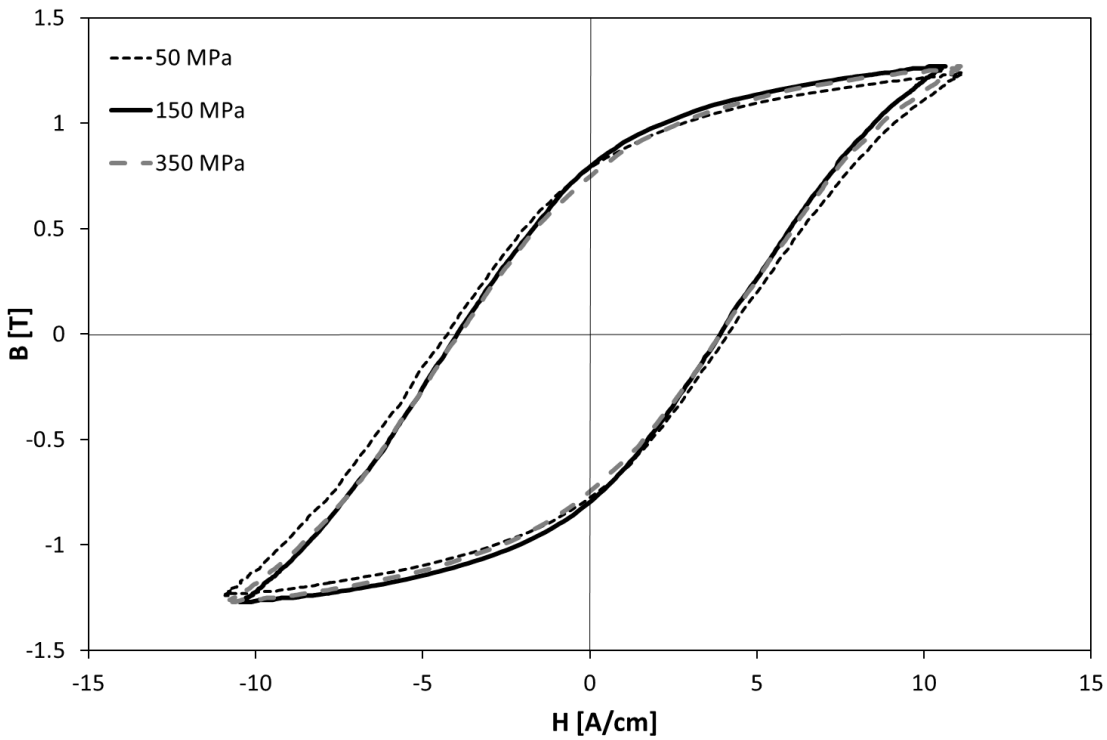

Figure 10 : Hysteresis curves under applied stress for non-deformed sample at 50, 150 and 350 MPa.

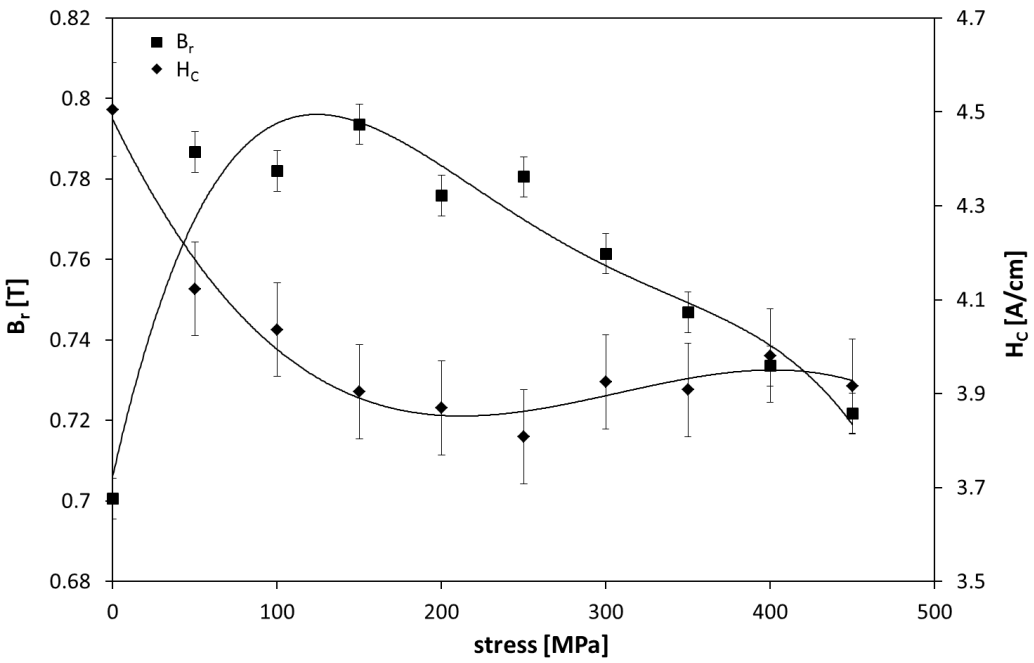

Figure 11 : Relation between remnant magnetic field (B_r) and coercive of magnetic field (H_C) derived from hysteresis curves with applied stress.

According to the Villari effect, mechanical stress changes the magnetic susceptibility which is directly related to the magnetization of the material [1]. Moreover, some studies suggested that the different shape of hysteresis loops under stress originates from the different sensitivities of 90° and 180° domain walls [1, 17], but some others named the effect of stress induced anisotropy as the main reason for this behavior [14, 18]. The second claim is in agreement with the observations made above and will be explained in the following. Equation 1 obtained from [2] shows the energy as a function of the crystal and stress anisotropy

$$E = K_1(\alpha_1^2\alpha_2^2 + \alpha_2^2\alpha_3^2 + \alpha_3^2\alpha_1^2) - \frac{3}{2}\lambda_{100}\sigma\,(\alpha_1^2\gamma_1^2 + \alpha_2^2\gamma_2^2 + \alpha_3^2\gamma_3^2) - \frac{3}{2}\lambda_{111}\sigma(\alpha_1\alpha_2\gamma_1\gamma_2 + \alpha_2\alpha_3\gamma_2\gamma_3 + \alpha_3\alpha_1\gamma_3\gamma_1) \quad \text{Eq.1}$$

where E, K_1, λ and σ are the energy, crystal anisotropy, saturation magnetostriction in a certain direction and applied stress, respectively. α and γ are the direction cosines of saturation magnetization (M_s) and stress (σ), respectively. The first term of equation 1 describes crystal anisotropy energy and the next two other terms are magnetoelastic energies. Therefore the equilibrium direction of M_s is that which makes E a minimum and which is largely influenced by the crystal anisotropy (K_1) and the stress anisotropy (K_σ). Stress anisotropy can be calculated using equation 2 [2].

$$K_\sigma = \frac{3}{2}\lambda_s \sigma \qquad \text{Eq. 2}$$

where λ_s is the saturation magnetostriction.

By using equations 1 and 2, the behavior of M_{MAX} under applied stress (σ) is described. Crystal anisotropy (K_1) is a constant parameter of the material, but stress anisotropy (K_σ) depends on applied stress and saturation magnetostriction. Figure 12 shows half of the magnetostriction curves at different applied stresses. As can be seen, the maximum magnetostriction λ_{MAX} decreases with increasing applied stress.

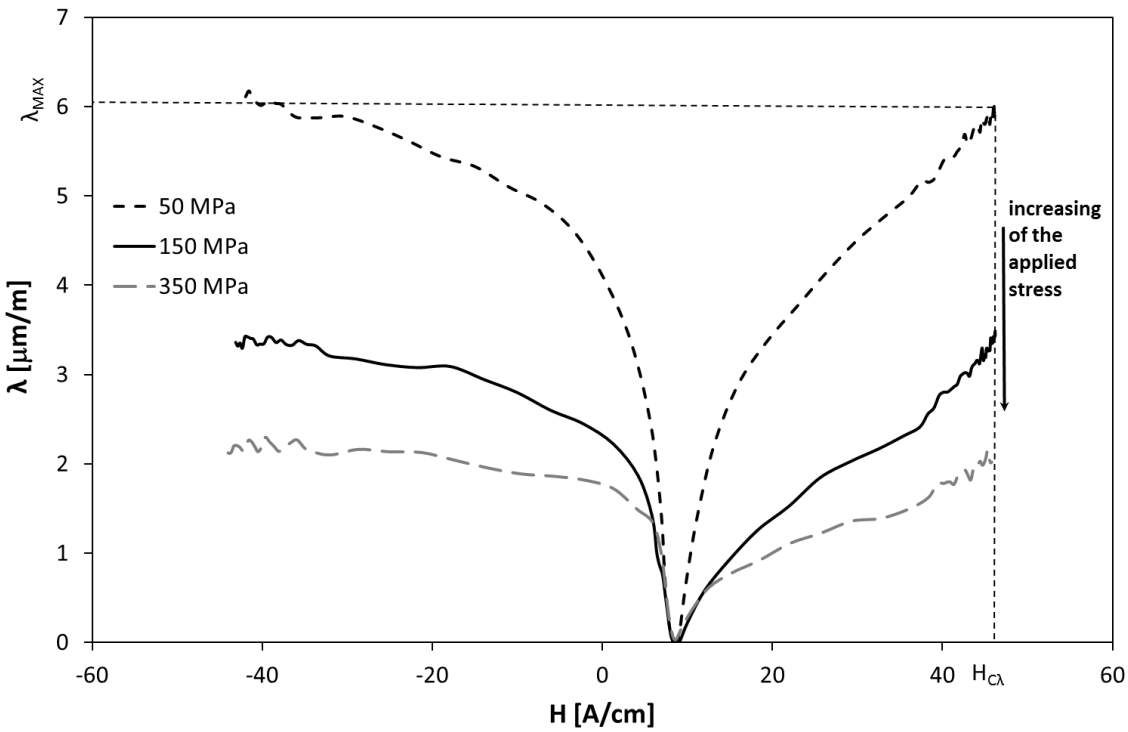

Figure 12 : Magnetostriction changes of non-deformed sample under applied stress at 50, 150 and 350 MPa.

Figure 13 shows the effect of applied stress on λ_{MAX} and K_σ where numbers have been taken from Figure 12 and calculated according to equation 2, respectively. Although λ_{MAX} decreases with increasing applied stress, K_σ increases. In other words, applied stress has a higher effect on K_σ rather than on λ_{MAX}.

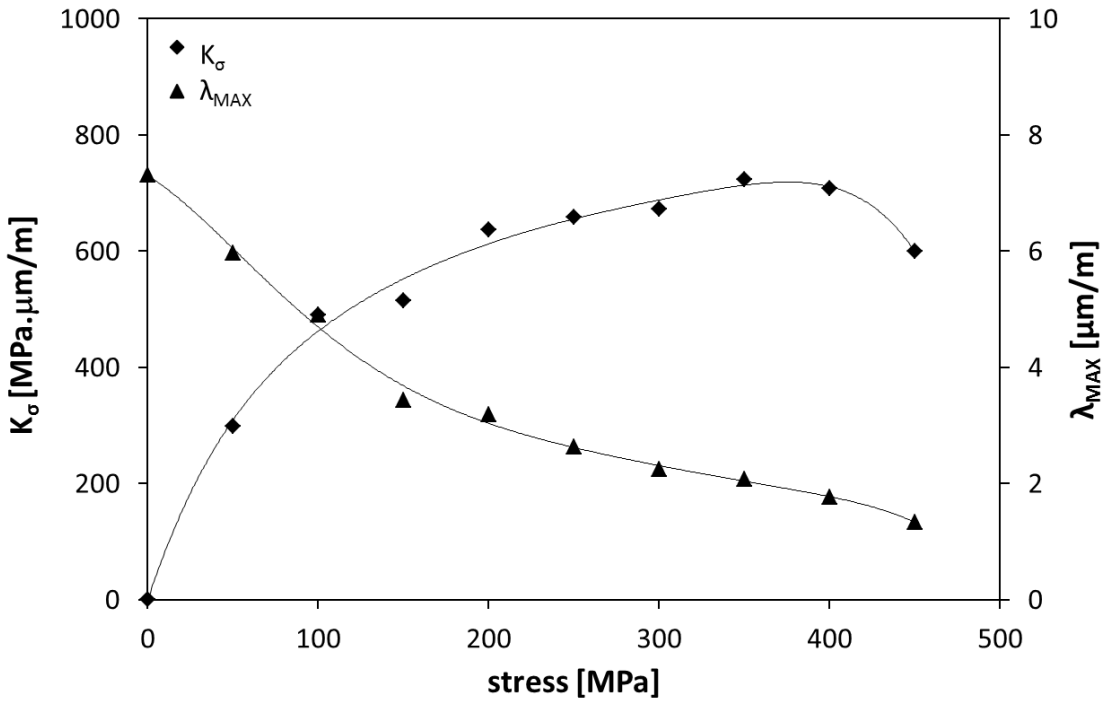

Figure 13: Effect of applied stress on maximum magnetostriction (λ_{MAX}) and stress anisotropy (K_σ).

Therefore there is a competition between two anisotropies to determine the magnetization easy axis under applied stress. At low applied stress, crystal anisotropy (K_1) is dominant, while at higher stresses, stress anisotropy (K_σ) plays the main role on the magnetization process. This means that in the case of the samples investigated at the applied stress values lower than 150 MPa, the easy axis is controlled by crystal anisotropy. Thus, domains turn into the direction of the magnetic easy axis which causes M_{MAX} to increase with increase of the applied stress. On the other hand, at higher applied stresses (higher than 150 MPa) stress anisotropy determines the magnetization easy axis which, for a material with positive magnetostriction, is in the direction of applied tensile stress. Therefore domains are forced to turn into the direction of the new easy axis which is controlled by stress [15]. To prove the above mentioned claim, a magnetic force microscope (MFM) was used to monitor magnetic domains at different applied stresses. Previously, electron backscatter diffraction (EBSD) and atomic force microscopy (AFM) were used to determine the grain orientation and roughness of the area marked on the specimen by FIB as mentioned before. Figure 14 shows the EBSD image of the marked area. As can be seen, most of the marked area is oriented in the direction of (111) especially at the down-left side of the picture.

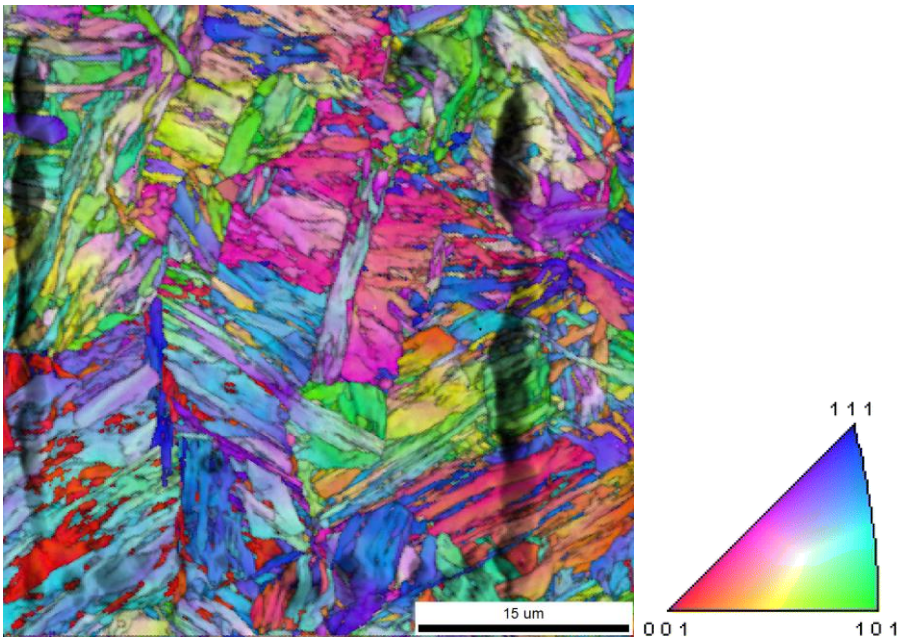

Figure 14: EBSD image of the marked area of the marked area.

Figure 15 shows domain structures at different applied stresses. It is noteworthy that higher contrasts come from the domains with opposite direction which are perpendicularly aligned to the surface while domains which are aligned parallel to the surface have lower contrast [19]. Growth of domains under applied stress in Figure 15a-d is the first change that is visible. Frequency analysis using two dimensional fast Fourier transformation (2D-FFT) was done on figure 15a and 15d to prove quantitatively growth of the domain structure under applied stress. Figure 16 demonstrates that Figure 15a has a more high frequency component than Figure 15d. Since the high frequency component comes from fine structure and vice versa for low frequency ones, Therefore, Figure 15a has finer domain structure than Figure 15d.

As can be seen in Figure 15 a-b, domain structures stay constant and just domains grow with increasing applied stress, while Figure 15 c-d show that the domains' structure changes gradually and some domains such as down-left side of the picture being oriented in (111) direction, grow in the direction of applied stress. This means that the domain structure at higher applied stresses higher than 150 MPa is different and tends to grow in applied stress direction. Therefore changes of domain structures beyond 150 MPa in applied stress causes the magnetization process to alter gradually which consequently affects MBN.

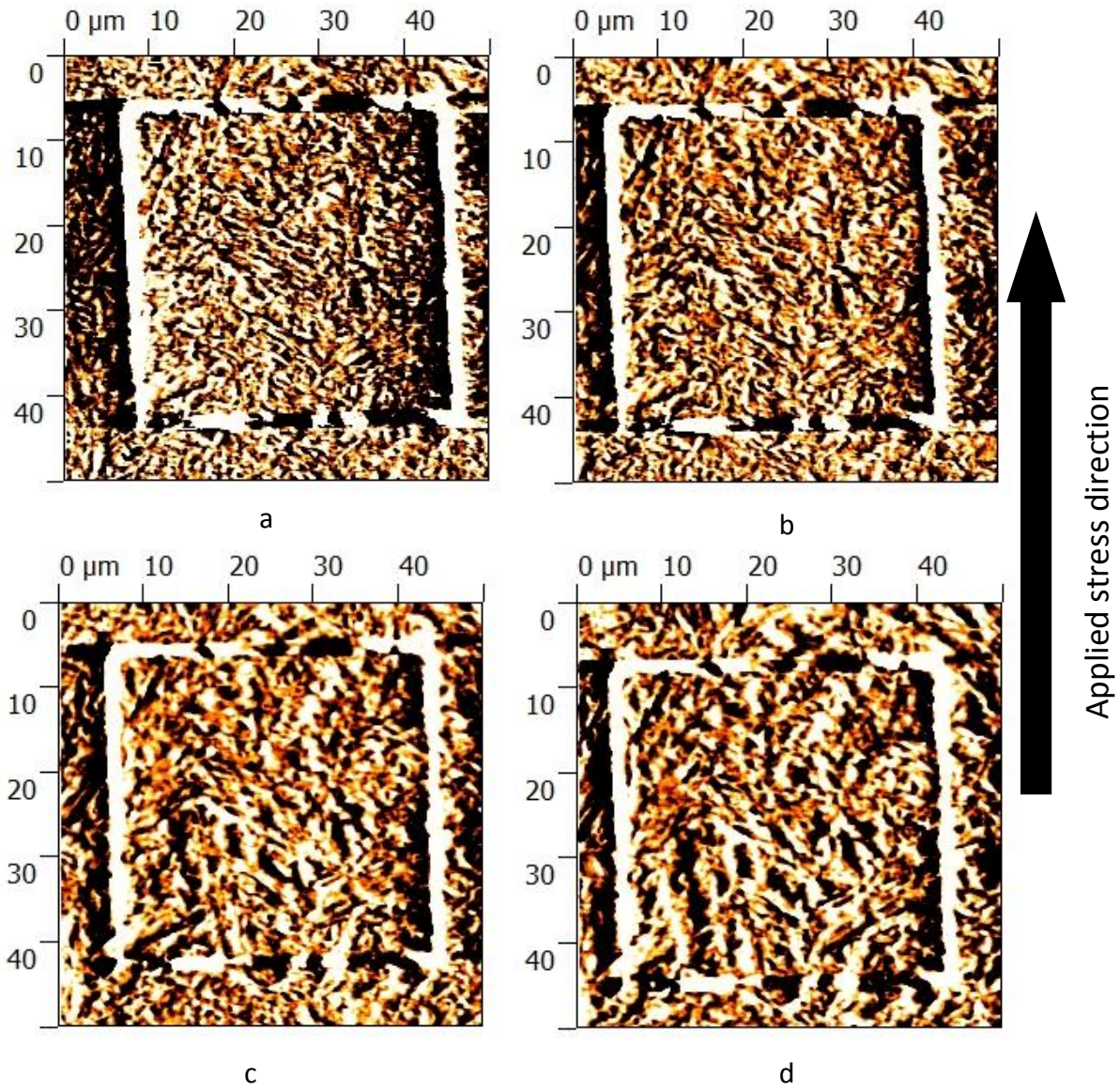

Figure 15: Domain structures under applied stress using magnetic force microscopy (MFM). a: 0MPa, b: 100MPa, c: 200MPa, d: 300MPa.

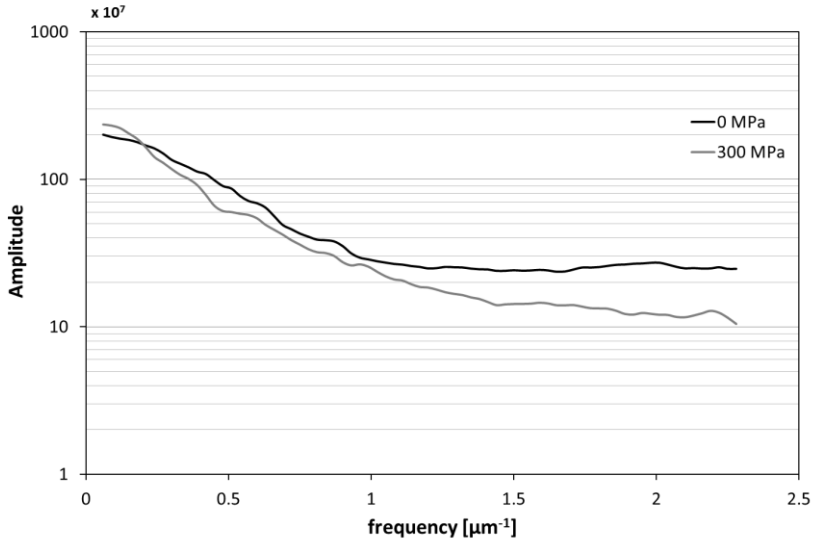

Figure 16: Two dimensional fast Fourier transformation (2D-FFT) on figures 15a and 15d.

4.3 Residual and applied stress

Figure 17 shows relationship between applied stress and M_{MAX} for non- and pre-deformed samples.

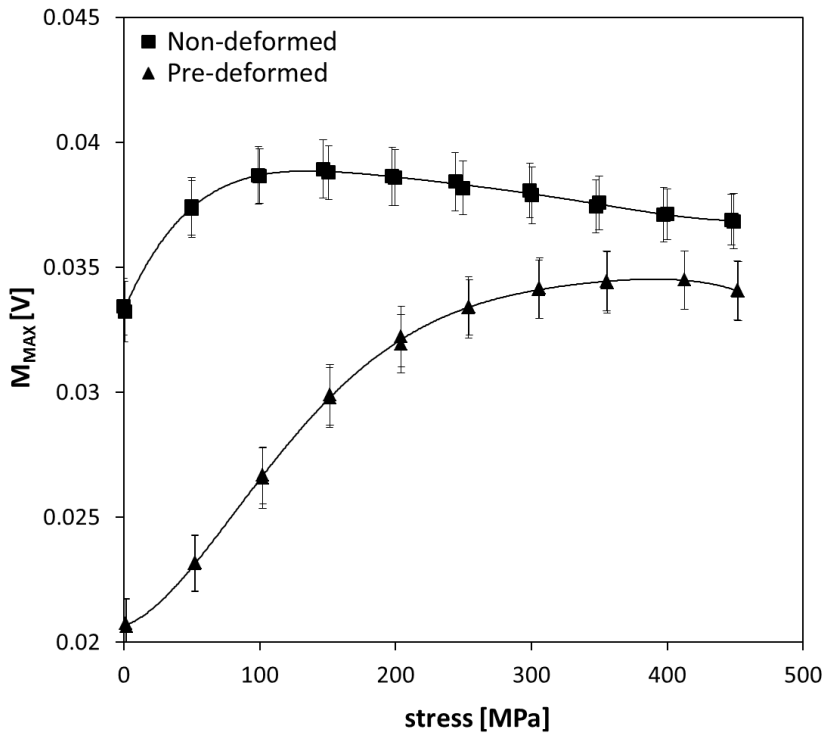

Figure 17 : Relation between maximum of Barkhausen noise (M_{MAX}) and applied stress for non- and pre-deformed samples.

In general, in the pre-deformed sample, due to micro compressive residual stresses, shows an overall smaller MBN compared to the non-deformed one [2, 3, 5]. Besides that, in the pre-deformed sample, $M_{MAX}(\sigma)$ curve reaches a peak at higher applied stress (around 400 MPa). It means that the stress anisotropy can dominate at higher applied stress in the competition to determine the magnetic easy axis because of the effect of micro compressive residual stresses which causes a hard magnetization axis in the direction of the applied stress [16]. In other words, three different anisotropies are active here: the crystal anisotropy (K_1), the stress anisotropy caused by the micro compressive residual stress ($K_{\sigma-}$), and the stress anisotropy caused by applied tensile stress ($K_{\sigma+}$). As far as the last two stress anisotropies are acting in opposite directions, therefore, the applied tensile stress should overcome a higher anisotropy for determining the magnetic easy axis. Thus the maximum of Barkhausen noise versus applied stress was detected at higher stress.

5. Conclusion

In this research the effect of micro residual and applied stress on MBN was studied. Strong evidence is provided for the existence of a competition between the crystal anisotropy (K_1) and the stress anisotropy (K_σ), which can therefore be assumed to play the main role in the determination of the magnetic easy axis. This claim was macroscopically approved using hysteresis and magnetostriction measurements. Also magnetic force microscopy was used to microscopically investigate the domain structures under applied stress. The results and consequently the influence of the applied stress for determining of the magnetic easy axis were further substantiated by the results of hysteresis and magnetostriction measurements.

6. References

[1] Bozorth R. M., “Ferromagnetism” IEEE Press, 1993, New York.

[2] Cullity B. D., Graham C. D., “Intruduction to magnetic materilas”, John Wiley press, 2009, Hoboken, New Jersey.

[3] Hauk V., “Structural and Residual Stress Analysis by Nondestructive Methods”, Elsevier, 1997, Amsterdam.

[4] Karjalainen L.P., Moilanen M., Rautioaho M., “Influence of tensile and cyclic loading upon Barkhausen noise in a mild steel”, Materials Evaluation, 37 (1979) 45-51.

[5] Jagadish C., Clapham L., Atherton D. L., “Influence of uniaxial elastic stress on power spectrum and pulse height distribution of surface Barkhausen noise in pipeline steel”, IEEE Transaction on magnetics, 26 (1993) 1160-1163.

[6] Stefanita C. G., Atherton D. L., Clapham L., “Plastic versus elastic deformation effects on magnetic Barkhausen noise in steel”, Acta Materialia, 48 (2000) 3545-3551.

[7] Sablik M.J., “A model for the Barkhausen noise power as a function of applied magnetic field and stress”, Journal of Applied Physics, 74 (1993) 5898-5900.

[8] Lindgren M. and Lepistö T., “Relation between residual stress and Barkhausen noise in a duplex steel”, NDT & E International, 36 (2003) 279-288.

[9] Lindgren M. and Lepistö T.: “On the stress vs. Barkhausen noise relation in duplex stainless steel”, NDT & E International, 37 (2004) 403-410.

[10] Kleber X. and Vincent A., “on the role of residual internal stresses and dislocations in Barkhausen noise in plastically deformed steel”, NDT & E International, 37 (2004) 439-445.

[11] Piotrowski L, Augustyniak B, Chmielewski M, Hristoforou E.V. and Kosmas K., “Evaluation of Barkhausen Noise and Magnetoacoustic Emission Signals Properties for Plastically Deformed Armco Iron” IEEE TRANSACTIONS ON MAGNETICS, 46 (2010) 239-242.

[12] Altpeter I., Dobmann G., Kröning M., Rabung M. and Szielasko S., “Micro-magnetic evaluation of micro residual stresses of the IInd and IIIrd order”, NDT & E International, 42 (2009) 283-290.

[13] Altpeter I., Becker R., Dobmann G. and Kern R., “Robust solutions of inverse problems in electromagnetic non-destructive evaluation”, Inverse Problems, 18 (2002) 1907-1921.

[14] Perevertov O., “Influence of the residual stress on the magnetization process in mild steel”, Journal of physics D: Applied physics, 40 (2007) 949-954.

[15] Perevertov O., Schäfer R., “Influence of applied compressive stress on the hysteresis curves and magnetic domain structure of grain-oriented transverse Fe-3%Si steel”, Journal of physics D: applied physics, 45 (2012) 135001.

[16] Szewczyka R., Bienkowskib A., “Application of the energy-based model for the magnetoelastic properties of amorphous alloys”, Journal of Magnetism and Magnetic Materials, 272–276 (2004) 728–730.

[17] Makar J.M., Tanner B.K., “The effect of plastic deformation and residual stress on the permeability and magnetostriction of steels”, Journal of Magnetism and Magnetic Materials, 222 (2000) 291-304.

[18] Anglada-Rivera J., Radovese L. R., Capo-Sanchez J., “Magnetic Barkhausen noise and hysteresis loop in commercial carbon steel: influence of applied tensile stress and grain size”, Journal of Magnetism and Magnetic Materials, 231 (2001) 299-306.

[19] Batista L., Rabe U., Altpeter I., Hirsekorn S., Dobmann G., “On the mechanism of nondestructive evaluation of cementite content in steels using a combination of

magnetic Barkhausen noise and magnetic force microscopy techniques", Journal of Magnetism and Magnetic Materials, 354 (2014) 248–256.